MODELING AND EXPERIMENTS OF THE HYSTERETIC RESPONSE OF AN ACTIVE HYDROFOIL ACTUATED BY SMA LINE ACTUATORS

D.C. Lagoudas, L.J. Garner, O.K. Rediniotis, and N. Wilson
Aerospace Engineering Department, Texas A&M University
College Station, Texas 77843-3141

1. Introduction

All movable control surfaces in surface ships and submarines, to date, involve a fixed stock (pivot axis) about which the appendage rotates. However, the location of the center of pressure on the appendage varies relative to the fixed stock over the range of angles of attack. The fundamental problem is that a parasitic and harmful hydrodynamic moment is created about the stock by the force-center being located some distance away from the stock centerline. Moreover, this force-center moves as the angle of attack changes. Preliminary research[1,2] indicates that a control surface with a small fraction (order of 10%) of its aft section being continuously deformed can move the center of pressure to just about any desired position on (or off) the surface, for a given angle of attack, thus controlling the torque about the primary stock. Early studies on Shape Memory Alloy (SMA) actuated control surfaces also indicated that large increases in the lift generated by the control surface could be attained via smooth deflection of the trailing edge.[3] It is possible to position the center of pressure such that there is zero parasitic torque on the primary stock while getting the equivalent lift as a traditional appendage. The use of active materials to effect the shape control can result in an all-electric actuation system without the noise associated with hydraulically moving mechanical components. Furthermore, optimal shape control will result in a hydrodynamically more efficient control surface, delaying or avoiding boundary layer separation, a phenomenon associated with shear layer shedding in the wake, a process which is acoustically harmful.

In actuator technology, active or "smart" materials have opened up new horizons in terms of actuation simplicity, compactness and miniaturization potential. Piezoelectric materials, Shape Memory Alloys, Magnetostrictive materials, Electrorheological Fluids (ERF) and Magnetorheological Fluids (MRF)[4] are the most often recognized types with the first three being the most common. These materials most commonly develop strains or, more applicably, displacements when exposed to electric, thermal and magnetic fields. Our experience with or knowledge of these material types indicates that SMAs are the most appropriate candidates for the present application where large forces and strains are required and the aquatic environment offers an ideal heat sink that will dramatically accelerate SMA actuation and increase actuation bandwidth. A few arguments to substantiate the appropriateness of SMAs are given below.

For the quasi-static or low-bandwidth applications of interest here (less than 2Hz), the high-frequency-response capabilities of piezoceramic and magnetostrictive materials (in the kHz range), are unnecessary and superfluous. Moreover, these materials are only capable of

producing small strains/displacements (measured in a few hundred microstrain) compared to those attained by SMA materials (as high as 8% for one-way trained and 4% for two-way trained SMAs).[5,6] SMAs provide the highest energy densities among the three active material types, as well as the highest stresses (up to 200 MPa). Additional SMA advantages include: (a) Simplicity of actuation mechanism. SMAs are all-electric devices and can be used as "Direct Drive Linear Actuators" with little or no additional gear reduction or motion amplification hardware. These merits permit the realization of small or even miniature actuation systems in order to overcome space limitation restrictions. Reduced production cost and improved reliability are other side benefits. (b) Silent actuation. Since no acoustic signature is associated with such an actuation system, acoustic detectability will be drastically reduced. (c) Low driving voltages. Nitinol (NiTi) SMAs can be actuated with very low voltages (5V to 12V), thus requiring very simple power driving hardware. In contrast, piezoceramic materials typically require voltages on the order of 100V for their actuation.

The tailoring and implementation of the accumulated knowledge into submersible vehicles is a task of multidisciplinary nature with two of the dominant fields being actuation and hydrodynamic control. Motivated by the ideas described above, an active hydrofoil with SMA actuators is being designed, modeled with FEA, and built for experimental validation. The active hydrofoil is modeled in the present work using a thermomechanical constitutive model for SMA coupled with a CFD code to model the hydrodynamic load. FEA has been performed and the model predictions have been compared with experimental measurements. The second section will give a more complete description of the active hydrofoil and its mode of operation. In the third section, the modeling of the hydrofoil in a fully-coupled hydro-mechanical environment is also discussed. Finally, a comparison of experimental results is drawn and the direction of ongoing work is discussed in the fourth section.

2. Description of the Active Hydrofoil

SMA actuator technology is presently applied to control the hydrodynamic forces and moments on a hydrofoil. The actuation elements are two sets of thin SMA wires attached to an elastomeric element that provides the main structural support and a hinge-less bend joint in the trailing edge of the hydrofoil. Controlled heating of the two wire sets generates bi-directional bending of the elastomer, which in turn deflects the trailing edge of the hydrofoil. The aquatic environment of the hydrofoil lends itself to cooling schemes that utilize the excellent heat transfer properties of water.

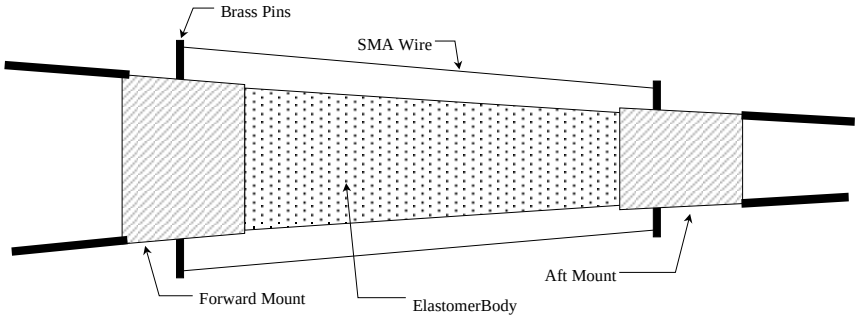

Figure 1. Schematic of hydrofoil center section

A schematic of the active hydrofoil is shown in Figure 1 and a photograph of the hydrofoil model can be seen in Figure 2. The model is comprised of three sections. The leading edge section encompasses the front of the model and is constructed of foam and fiberglass. This section is hollow to allow the mounting of the pitch sensor within the model. This section also has a shaft passing through it upon which the model is mounted in the water tunnel as shown in Figure 3. The bearings and the exit point on the shaft are waterproofed before the model is submerged. The wires for the on-board inclinometers and thermocouples also pass through the leading edge section and then out of the model through the mounting shaft. Attached to the rear of the leading edge section is the SMA-actuator. The elastomer is mounted in a Plexiglas frame that is fastened to the leading-edge section. The trailing edge, which is also constructed out of fiberglass, is attached to the elastomer in a similar fashion. In order for the model to balanced, fore and aft, about the shaft, lead weights are added to the hollow area in the leading-edge section of the model. Balancing weights are also added to make the model neutrally buoyant.

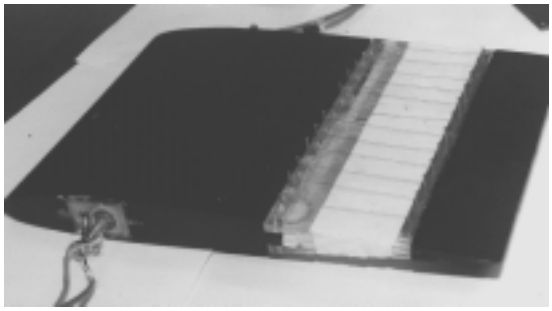

Figure 2. Photograph of the active hydrofoil showing placement of SMA wires.[7]

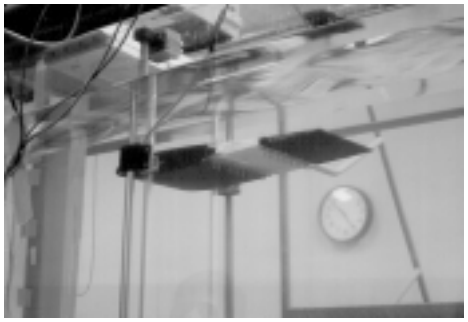

Figure 3. Water tunnel setup with hydrofoil.

The SMA actuator consists of a SMA wire that has been conditioned to acquire a two-way shape memory effect, so that the wire can change as much as 3.5% in length during a temperature cycle. The positioning of the SMA wires is such that when the wires on the upper surface are heated by electrical current, the trailing edge is deflected up. By having the wire exposed directly to the water flow, the maximum possible cooling rate can be achieved.

3. Finite Element Modeling of an Active Hydrofoil

A constitutive model for SMA, which will be discussed later, has been developed and has been successfully integrated into the commercial Finite Element program ABAQUS. Using this constitutive model and ABAQUS, it is possible to model fully coupled thermomechanical problems or the mechanical response to a specified temperature variation. In the current analysis, the temperature of the SMA is taken from experimental measurements in order to reduce computational time and simplify the model. Figure 4 shows a finite element mesh of the hydrofoil trailing edge model. This three-dimensional model exploits the spanwise periodicity of the design by modeling only one cell (section between two adjacent SMA wires) of the hydrofoil and consists of the center and aft sections of the hydrofoil only. This model was used to correlate with in air tests of the hydrofoil. The SMA wires are represented by one-dimensional truss elements rigidly fixed to planar elements representing the pins on the ends. The elastomer is represented by 20-node brick elements. Also shown in Figure 4 is the deflected hydrofoil mesh at maximum deflection, with the bottom set of wires actuated.

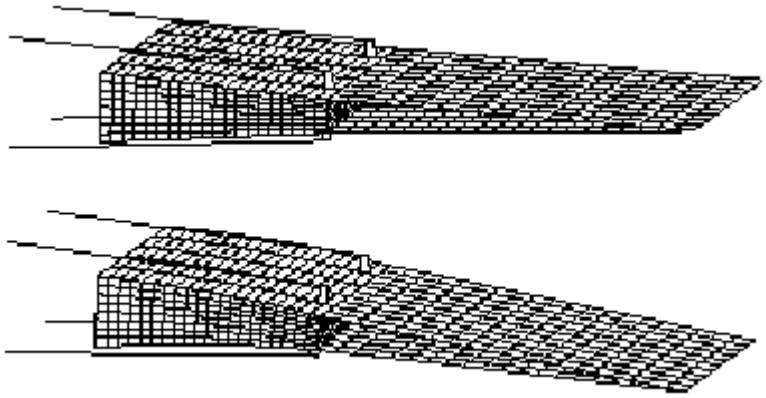

Figure 4. Finite Element mesh of hydrofoil trailing edge and the deformed mesh at maximum deflection.

In order to model the hydro-mechanical coupling the FEM model mesh need to be expanded to include the entire airfoil surface. Also, results showed the variation in stress along the span caused by periodic arrangement of the SMA actuators is negligible. Therefore, the mesh was reduced to a two-dimension constructed of plane strain elements with the same truss elements representing the SMA.

3.1. MODELING OF HYDRO-MECHANICAL COUPLING

The nature of the aquatic environment introduces substantial hydrodynamic loads to the analysis. These loads are dependent of the deflection of the hydrofoil trailing edge. This dependency creates a strong coupling between the hydrodynamic loads and the mechanical response. An iterative procedure was developed to model the coupling between the hydrodynamic forces and the mechanical response of the hydrofoil. In this procedure, shown in Figure 5, the SMA wires are actuated in the absence of hydrodynamic forces, resulting in the maximum possible deflection of the hydrofoil trailing edge. For this deflected shape, the hydrodynamic forces are evaluated and are used to modify the loading boundary conditions for the mechanical problem. A new deflected shape is evaluated by the modified FEA and the hydrodynamic forces are computed again for the updated shape. This iterative procedure is complete when the difference in the lift coefficient between consecutive iterations becomes smaller than a given tolerance.

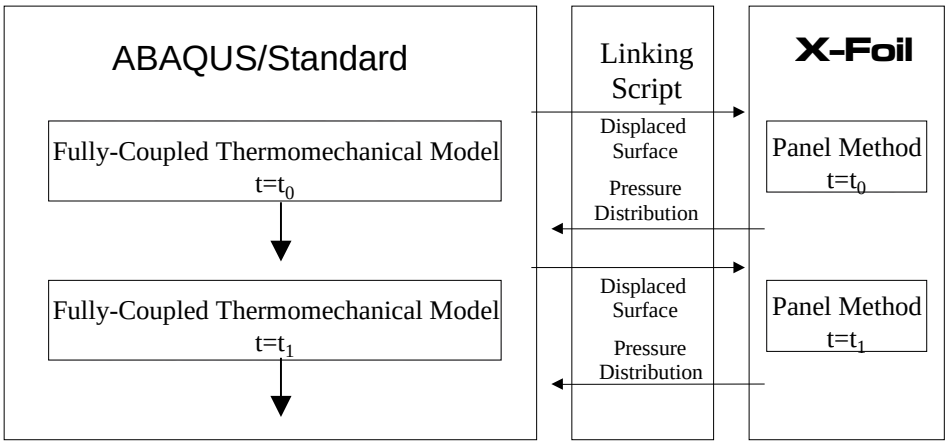

Figure 5. Schematic of hydro-mechanical coupling procedure.

Since the FEM model can only track displacements at nodes, this is the only data that can be supplied to the panel method to describe the airfoil shape. In order to produce good results the panel method requires fine resolution of the leading and trailing edges. This requires the placement of many nodes on the leading and trailing edges in the FEM model. Since these areas have very low stress gradients and are not of structural interest, this is a great penalty. While it is true that leading and trailing edges are essentially rigid bodies, their presence in the FEM model is required in order to accurately calculate hydrodynamic forces and moments. Also, the nodes comprising the upper and lower surface will not remain vertically aligned as the airfoil deforms the panel methods. This problem leads to more inaccuracy and creates a blunt trailing edge. The use of Xfoil (a 2-D panel method CFD code with boundary layer capabilities[8]) eliminates both of these problems by creating its own model of the hydrofoil based on coordinates supplied. It is therefore only required to provide enough

nodal coordinates to accurately describe the airfoil shape. Xfoil is also able to accurately calculate the pressures for airfoils with blunt trailing edges.

Figure 6 shows the predicted deflection of the trailing edge for a freestream velocity of 1ft/sec. It should be noted that while ignoring the hydrodynamic load produces only small errors in displacement, the error in the predicted lift is substantial. Also shown in the figure is the convergence of the lift coefficient.

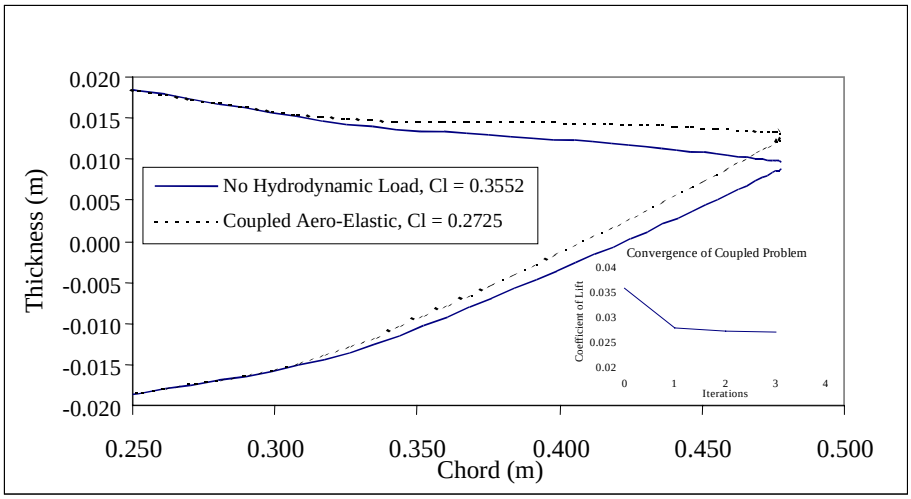

Figure 6. Hydrofoil trailing edge deflection showing the effect of hydrodynamic forces and rate of convergence of the iterative coupling scheme.

3.2. SMA CONSTITUTIVE MODEL

For the numerical simulation of this problem, the 3-D incremental formulation of the SMA constitutive model, developed by Boyd and Lagoudas[9], is used to predict the thermomechanical response of SMA. The model consists of three sets of equations: The constitutive equations, which describe the increment of strain, in terms of the increments of stress, temperature, and the volume fraction of martensite, $\dot{\sigma}_{ij}, \dot{T}, \dot{\xi}$ respectively. i.e.,

$$\dot{\varepsilon}_{ij} = S_{ijkl}\dot{\sigma}_{kl} + \alpha_{ij}\dot{T} + Q_{ij}\dot{\xi} \tag{1}$$

the transformation equation, which relates the increment of martensite volume fraction to the transformation strain, i.e,

$$\dot{\varepsilon}^{t}_{ij} = \Lambda_{ij}\dot{\xi} \tag{2}$$

and the transformation surface equation, which controls the onset of the forward and reverse phase transformations, i.e.,

$$\pi = \sigma_{ij}^{eff}\Lambda_{ij} + \frac{1}{2}\Delta S_{ijkl}\,\sigma_{ij}\sigma_{kl} + \Delta\alpha_{ij}\sigma_{ij}\Delta T + \rho\,\Delta c\left[\Delta T - T\ln\left(\frac{T}{T_o}\right)\right]$$
$$+ \rho\,\Delta s_o T - b\xi - \mu_1 \pm \frac{1}{4}\Delta\rho\, b - \rho\,\Delta u_o = \pm Y^* \tag{3}$$

The plus sign on the right hand side in Eq. (3) should be used for the forward phase transformation (austenite to martensite), while the minus sign should be used for the reverse phase transformation (martensite to austenite). Note that the material constant Y^* can be interpreted as the threshold value of the transformation surface, π, for the onset of the phase transformation.

In the above equations $S_{ijkl}=(C_{ijkl})^{-1}$ is the elastic compliance tensor, α_{ij}, is the thermal expansion coefficient tensor, given in terms of the volume fraction of martensite by

$$C_{ijkl} = C_{ijkl}^{A} + \xi\left(C_{ijkl}^{M} - C_{ijkl}^{A}\right)$$
$$\alpha_{ij} = \alpha_{ij}^{A} + \xi\left(\alpha_{ij}^{M} - \alpha_{ij}^{A}\right) \tag{4}$$

where the superscripts "A" and "M" denote the austenitic and martensitic phases, respectively. The various other terms in Eqs. (1)- (3) are defined by

$$Q_{ij} = \Delta S_{ijkl}\,\sigma_{kl} + \Delta\alpha_{ij}\left(T - T_o\right) + \Lambda_{ij}$$
$$\Lambda_{ij} = \begin{cases} \frac{3}{2}H\left(\bar{\sigma}^{eff}\right)^{-1}\sigma_{ij}^{eff}{}', & \dot{\xi} > 0 \\ H\left(\bar{\varepsilon}^{t}\right)^{-1}\varepsilon_{ij}^{t}, & \dot{\xi} < 0 \end{cases}$$
$$\bar{\sigma}^{eff} = \left(\frac{3}{2}\sigma_{ij}^{eff}{}'\sigma_{ij}^{eff}{}'\right)^{\frac{1}{2}}, \qquad \sigma_{ij}^{eff}{}' = \sigma_{ij}^{eff} - \frac{1}{3}\sigma_{kk}^{eff}\delta_{ij} \tag{5}$$
$$\bar{\varepsilon}^{t} = \left(\frac{3}{2}\varepsilon_{ij}^{t}\varepsilon_{ij}^{t}\right)$$

Note that $H=\varepsilon^{t,max}$ corresponds to the maximum uniaxial transformation strain and is found from uniaxial stress-strain curve for detwinning of martensite at temperatures below M_0^S. The remaining terms that are defined with the prefix "Δ" indicate the difference of a quantity between the austenitic and martensitic phase , and are given by

$$
\begin{aligned}
\Delta S_{ijkl} &= \frac{\partial S_{ijkl}}{\partial \xi} = -\left(S_{ijpq}\right) \Delta C_{pqmn} \left(S_{mnkl}\right) \\
\Delta C_{ijkl} &= C^{M}_{ijkl} - C^{A}_{ijkl}, \qquad \Delta \alpha_{ij} = \alpha^{M}_{ij} - \alpha^{A}_{ij} \\
\Delta c &= c^{M} - c^{A}, \qquad \Delta s_{o} = s^{M}_{o} - s^{A}_{o} \\
\Delta u_{o} &= u^{M}_{o} - u^{A}_{o}, \qquad \Delta T = T - T_{o} \\
\Delta \rho b &= \rho b^{A} - \rho b^{M}
\end{aligned}
\tag{6}
$$

where ρ, c, $s_{o,}$ u, b are the mass density, specific heat, specific entropy, specific internal energy at the reference state, and the transformation strain hardening constant, respectively.

The hardening function, $f(\xi)$, describes transformation induced strain hardening in the SMA material and is given by

$$
f(\xi) = \begin{cases} f^{M0}(\xi) + \dfrac{1-\xi}{1-\xi^{R}}\left[\left(f^{A}\left(\xi^{R}\right) - f^{M0}\left(\xi^{R}\right)\right)\right] \\ f^{A0}(\xi) + \dfrac{\xi}{\xi^{R}}\left[\left(f^{M}\left(\xi^{R}\right) - f^{A0}\left(\xi^{R}\right)\right)\right] \end{cases}
\tag{7}
$$

where

$$
\begin{aligned}
f^{M0}\left(\xi\right) &= \frac{1}{2}\rho b \xi^{2} + \left(\mu_{1} + \mu_{2}\right)\xi \\
f^{A0}\left(\xi\right) &= \frac{1}{2}\rho b \xi^{2} + \left(\mu_{1} - \mu_{2}\right)\xi
\end{aligned}
\tag{8}
$$

and ξ^{R} is the martensitic volume fraction at a point during the phase transformation characterized by a change in the sign of $\dot{\xi}$. The material constants μ_1, μ_2, are used to describe the accumulation of the elastic strain energy at the onset of the forward phase transformation and to enforce the continuity of $f(\xi)$ at $\xi = 1$, respectively.

The implementation of the incremental SMA constitutive model is performed using incremental Newton-Raphson iteration method based on displacement formulation. The scheme requires the tangent stiffness tensor and the stress tensor at each integration point to be updated in each iteration for given increments of strain and temperature. In order to obtain the stress tensor and tangent stiffness, the transformation function Φ is defined using Eq. (1) as follows[10]

$$
\Phi = \begin{cases} \pi - Y^{*}, & \dot{\xi} > 0 \\ -\pi - Y^{*}, & \dot{\xi} < 0 \end{cases}
\tag{9}
$$

The forward phase transformation (austenite to martensite) is characterized by $\Phi = 0$ and $\dot{\xi} > 0$, while the reverse phase transformation (martensite to austenite) is

characterized by $\Phi = 0$ and $\dot{\xi} < 0$. Using the consistency condition $\dot{\Phi} = 0$, the evolution of the martensitic volume fraction can be derived. Substituting this result into the stress rate form of Eq.(1), the tangent stiffness tensor L_{ijkl} and tangent thermal moduli l_{ij} are given by

$$L_{ijkl} = C_{ijkl} + \frac{1}{B} C_{ijmn} Q_{mn} R_{kl}, \quad l_{ij} = C_{ijkl}\left(Q_{kl} \frac{S}{B} - \alpha_{kl} \right)$$

$$R_{kl} = C_{ijkl} \frac{\partial \Phi}{\partial \sigma_{ij}}, \quad B = \frac{\partial \Phi}{\partial \xi} - \frac{\partial \Phi}{\partial \sigma_{pq}} C_{pqrs} Q_{rs} \tag{10}$$

$$S = \frac{\partial \Phi}{\partial T} - \frac{\partial \Phi}{\partial \sigma_{ij}} C_{ijkl} Q_{kl}$$

To calculate the increment of stress for given strain and temperature increments according to SMA constitutive model, a return mapping integration algorithm proposed by Ortiz and Simo[11] has been used. The work by Lagoudas *et. al.*[10] can be consulted for details of the implementation.

4. Comparison of Experimental and FEM Model Results

The SMA wires used in the model were previously trained using thermal cycles under constant applied stress. The material constants used in the model were obtained is a series of test performed by cycling the temperature under constant load. These tests were used to determine the transformation temperatures, (M_0^F, M_0^S, A_0^S, A_0^F) and the slopes of the transformation boundaries as seen on a stress temperature plot. These parameters as well as the amount of pre-strain (training) were also used as input to the model. In order to obtain properties for the elastomer, the hydrofoil was subjected to a known load on the tip with the hydrofoil body being rigidly fixed and the SMA wires being removed. The deflection of the tip was measured and used to calibrate the FEM model of the hydrofoil structure.

The results of a low frequency test in air are shown in Figure 7. In-air testing is done to verify the FEM model without hydrodynamic forces being present. For this test, the hydrofoil is again clamped and the upper set of SMA wires are heated by electrical current. The wire temperature and the deflection of the trailing edge are measured and shown in the figure. The test time was protracted to allow the thermocouples sufficient time to assure accurate measurement of temperature. Prior to the application of the temperature profile the hydrofoil was cooled to –20°C to assure an all martensite initial state. The temperature profile shown (experimentally measured) was used as an input to the analysis. The tip deflection predicted by the FEA using the temperature profile from the experiment is also shown in the figure. As is seen in the figure, reasonable agreement between the model and experiment was achieved.

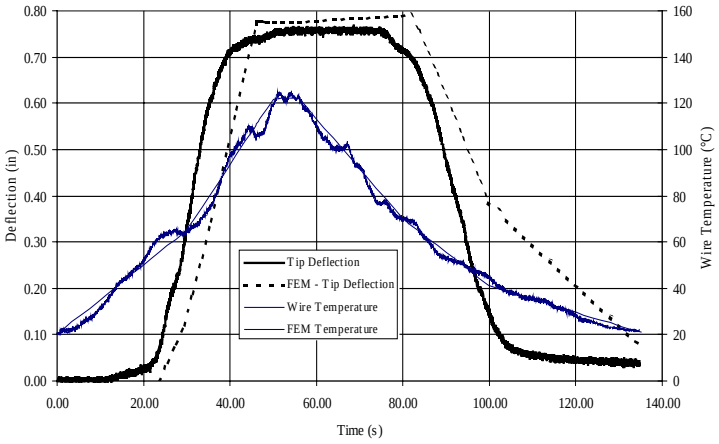

Figure 7. Experimental and numerical hydrofoil (trailing edge) tip deflection and wire temperature versus time for quasi-static actuation in still air.

Tests of the hydrofoil in the water tunnel were also preformed. Figure 8 shows the results of water tunnel tests at two flow velocities and the results from the in-air test described above. The data shown are the tip deflection plotted against the SMA wire temperature. As can be seen in the figure there is a large change in the tip deflection when the hydrofoil is submerged. This change can be attributed to the combination of much larger heat transfer which prevents the wires from being able to be heated sufficiently to cause complete transformation and the shift in the transition temperatures due to the increased load of the hydrodynamic forces. The change in the transition temperatures due to increased load can be seen in the figure in the shift of the hystersis loops to the right as the flow speed increases. The figure also shows that the temperature measured by the thermocouples becomes unreliable as the velocity of the flow increases.

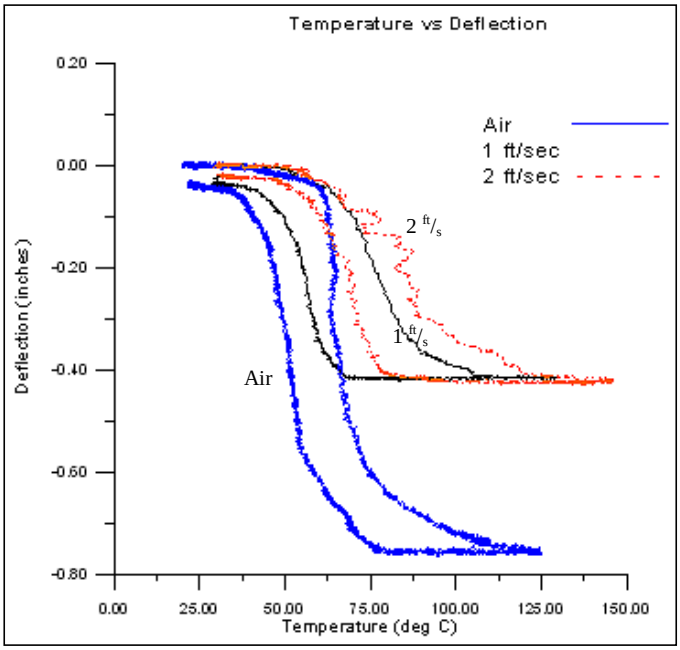

Figure 8. Hydrofoil experimental test results comparing trailing edge deflection vs., wire temperature of hydrofoil in air and in water tunnel at two fluid velocities.

The results of these hydrofoil tests in the water tunnel identified several difficulties in modeling the response of the hydrofoil in this complex environment. (1) Since the martensitic finish temperature of the wire was below the temperature of the water tunnel, full reverse transformations are not possible. This creates uncertainty in the initial state of the martensitic volume fraction of subsequent temperature cycles. (2) The thermocouples attached to the wires are exposed to the flow and register a temperature, which is influenced by the temperature of the water. This renders the experimental measurement of the wire temperature unreliable. This difficulty will require using the fully-coupled thermomechanical model. (3) The control surface needs to be able to deflect through a full range of positions. The ability to model minor loops (partial transformations) is desired. (4) The amount of load on the SMA in this configuration is dependent on the amount of deflection. A more advanced material model capable of modeling non-proportional loading is needed.

Work is currently underway to resolve these difficulties. The solutions to these problems are as follows. (1)New Ni-Ti-Cu wire have been obtained which have martensitic finish temperatures above 30°C. (2)Both the SMA constitutive model and the FEM program are capable of modeling fully-coupled thermomechanical problems. The hydrofoil response will be modeled as a function of the electrical current supplied to the SMA wire actuators. (3)A new SMA constitutive model which is capable of modeling minor loops has been

developed by Bo and Lagoudas and implemented in the FEM code.[12] (4)The new constitutive model by Bo and Lagoudas can accurately model SMA under non-proportional loading.

5. Acknowledgements

The authors wish to acknowledge the financial support of this research by the Office of Naval Research, Contract No. N00014-97-1-0840 and Aeroprobe Corporation, Project No. 96-386.

---

[1] HE&D, Inc. 1990, "FACS: Flap Assisted Control Surface," Progress Report, Arlington, Virginia.

[2] Traub, L.W., Singh, K., Aguilar, V., Kim, K. and Rediniotis, O.K., 1996, "Conceptual Analysis of a Flap Assisted Control Surface," Texas A&M University, College Station, Texas.

[3] Beauchamp, C., Nadolink, R, and Dean, L., 1992, "Shape Memory Alloy Articulated (SMAART) Control Surfaces), *SPIE Conf, ActiveMaterials and Adaptive Structures – Session 25*.

[4] Giurgiutiu, V., Chaudhry, Z., Rogers, C.A., 1994, "The Analysis of Power Delivery Capability of Induced-Strain Actuators for Dynamic Applications", Proc. Second International Conf. On Intelligent Materials, ICIM '94, Colonial Williamsburg, VA, Technomic Pub. Co.

[5] Jackson, C.M., Wagner, H.J., and Wasilewski, R.J., 1972, "55-Nitinol – The Alloy with a Memory: Its Physical Metallurgy, Properties, and Applications, Technical Report", NASA-SP 5110.

[6] Hodgson, D. , 1988, *Using Shape Memory Alloys*, Shape Memory Alloy Applications, Sunnyvale, CA

[7] Rediniotis, O.K., Lagoudas, D.C., Garner, L. and Wilson, N., 1998, "Experiments and Analysis of an Active Hydrofoil with SMA Actuators," AIAA Paper No. 98-0102, 36th AIAA Aerospace Sciences Meeting, Reno, Nevada.

[8] Drela, M., 1996, "Xfoil 6.8 User Primer", MIT Aero &Astro.

[9] Boyd, J.G., and Lagoudas, D.C., 1996, "A Thermodynamical Constitutive Model for Shape Memory Materials. Part I. The Monolithic Shape Memory Alloy," *International Journal of Plasticity* (in print).

[10] Lagoudas, D.C., Bo, Z., and Qidwai, M.A., 1996, "A Unified Thermodynamic Constitutive Model for SMA and Finite Element Analysis of Active Metal Matrix Composites," *Mechanics of Composite Materials and Structures*, Vol.4, pp. 153-179.

[11] Ortiz, M. and Sumo, J.C., 1986, "An Analysis of a New Class of Integration Algorithms for Elastoplastic Constitute Relations", *International Journal for Numerical Methods in Engineering*, Vol. 23 pp. 353-366

[12] Bo, Z., Lagoudas, D., and Miller, D., 1998, "Material Characterization of SMA Actuators under Non-Proportional Thermomechanical Loading", submitted to JEMT Special Edition on SMA.